



3D-Printed Biohybrid Microstructures Enable Transplantation and Vascularization of Microtissues in the Anterior Chamber of the Eye

Kavand, H., Visa, M., Köhler, M., van der Wijngaart, W., Berggren, P-O., & Herland, A. (2023). 3D-Printed Biohybrid Microstructures Enable Transplantation and Vascularization of Microtissues in the Anterior Chamber of the Eye. *Advanced Materials*, Article e2306686. Advance online publication. <https://doi.org/10.1002/adma.202306686>

[Link to publication record in Ulster University Research Portal](#)

Published in:
Advanced Materials

Publication Status:
Published online: 10/10/2023

DOI:
[10.1002/adma.202306686](https://doi.org/10.1002/adma.202306686)

Document Version
Publisher's PDF, also known as Version of record

General rights
Copyright for the publications made accessible via Ulster University's Research Portal is retained by the author(s) and / or other copyright owners and it is a condition of accessing these publications that users recognise and abide by the legal requirements associated with these rights.

Take down policy
The Research Portal is Ulster University's institutional repository that provides access to Ulster's research outputs. Every effort has been made to ensure that content in the Research Portal does not infringe any person's rights, or applicable UK laws. If you discover content in the Research Portal that you believe breaches copyright or violates any law, please contact pure-support@ulster.ac.uk.

3D-Printed Biohybrid Microstructures Enable Transplantation and Vascularization of Microtissues in the Anterior Chamber of the Eye

Hanie Kavand, Montse Visa, Martin Köhler, Wouter van der Wijngaart,*
Per-Olof Berggren,* and Anna Herland*

Hybridizing biological cells with man-made sensors enable the detection of a wide range of weak physiological responses with high specificity. The anterior chamber of the eye (ACE) is an ideal transplantation site due to its ocular immune privilege and optical transparency, which enable superior noninvasive longitudinal analyses of cells and microtissues. Engraftment of biohybrid microstructures in the ACE may, however, be affected by the pupillary response and dynamics. Here, sutureless transplantation of biohybrid microstructures, 3D printed in IP-Visio photoresin, containing a precisely localized pancreatic islet to the ACE of mice is presented. The biohybrid microstructures allow mechanical fixation in the ACE, independent of iris dynamics. After transplantation, islets in the microstructures successfully sustain their functionality for over 20 weeks and become vascularized despite physical separation from the vessel source (iris) and immersion in a low-viscous liquid (aqueous humor) with continuous circulation and clearance. This approach opens new perspectives in biohybrid microtissue transplantation in the ACE, advancing monitoring of microtissue–host interactions, disease modeling, treatment outcomes, and vascularization in engineered tissues.

real-time measuring arterial pressure and pulse rate,^[1] neuronal activities,^[2,3] glucose monitoring,^[4] and intraocular pressure (IOP).^[5] However, biosensors composed of living cells as a part of their sensing element, known as biohybrid sensors, are considered superior to biosensors that exclusively depend on physicochemical changes near the sensor. This is because the biological unit in biohybrid sensors can sense and respond to a wider range of weak physiological stimuli with higher specificity^[6] and can integrate with the host through vascularization to create a more physiological connection to the external evaluation units. Recent in vitro studies have shown the potential of biohybrid sensors for applications such as odorant^[7] and taste^[8] sensing, directional chemical source detection,^[9] infrared detection,^[10] and drug evaluation.^[11,12] However, to extend these applications to in vivo microenvironments, new strategies are needed that can meet the requirements of the host tissue, the biological sensing,

and the nonbiological readout units.


We have developed a microstructure that can both securely hold a microtissue in a specific location within the ACE and promote tissue engraftment (**Figure 1**). We chose pancreatic islets as the model microtissue due to their importance and

1. Introduction

The development of implantable biomedical sensors is moving toward real-time in vivo screening. Sensors based on electrical, mechanical, or optical modules have been developed for

H. Kavand, W. van der Wijngaart, A. Herland
Division of Micro- and Nanosystems
Department of Intelligent Systems
KTH Royal Institute of Technology
Malvinas Väg 10 pl 5, Stockholm SE-10044, Sweden
E-mail: wouter@kth.se; aherland@kth.se

H. Kavand, A. Herland
Division of Nanobiotechnology
Department of Protein Science
KTH Royal Institute of Technology
Tomtebodavägen 23a, Stockholm SE-17165, Sweden
M. Visa, M. Köhler, P.-O. Berggren
The Rolf Luft Research center for Diabetes and Endocrinology
Karolinska Institutet
Stockholm SE-17176, Sweden
E-mail: per-olof.berggren@ki.se
A. Herland
AIMES
Center for the Advancement of Integrated Medical and Engineering Sciences
Department of Neuroscience
Karolinska Institutet
Solnavägen 9/B8, Stockholm SE-17165, Sweden

 The ORCID identification number(s) for the author(s) of this article can be found under <https://doi.org/10.1002/adma.202306686>

© 2023 The Authors. Advanced Materials published by Wiley-VCH GmbH. This is an open access article under the terms of the Creative Commons Attribution-NonCommercial License, which permits use, distribution and reproduction in any medium, provided the original work is properly cited and is not used for commercial purposes.

DOI: 10.1002/adma.202306686

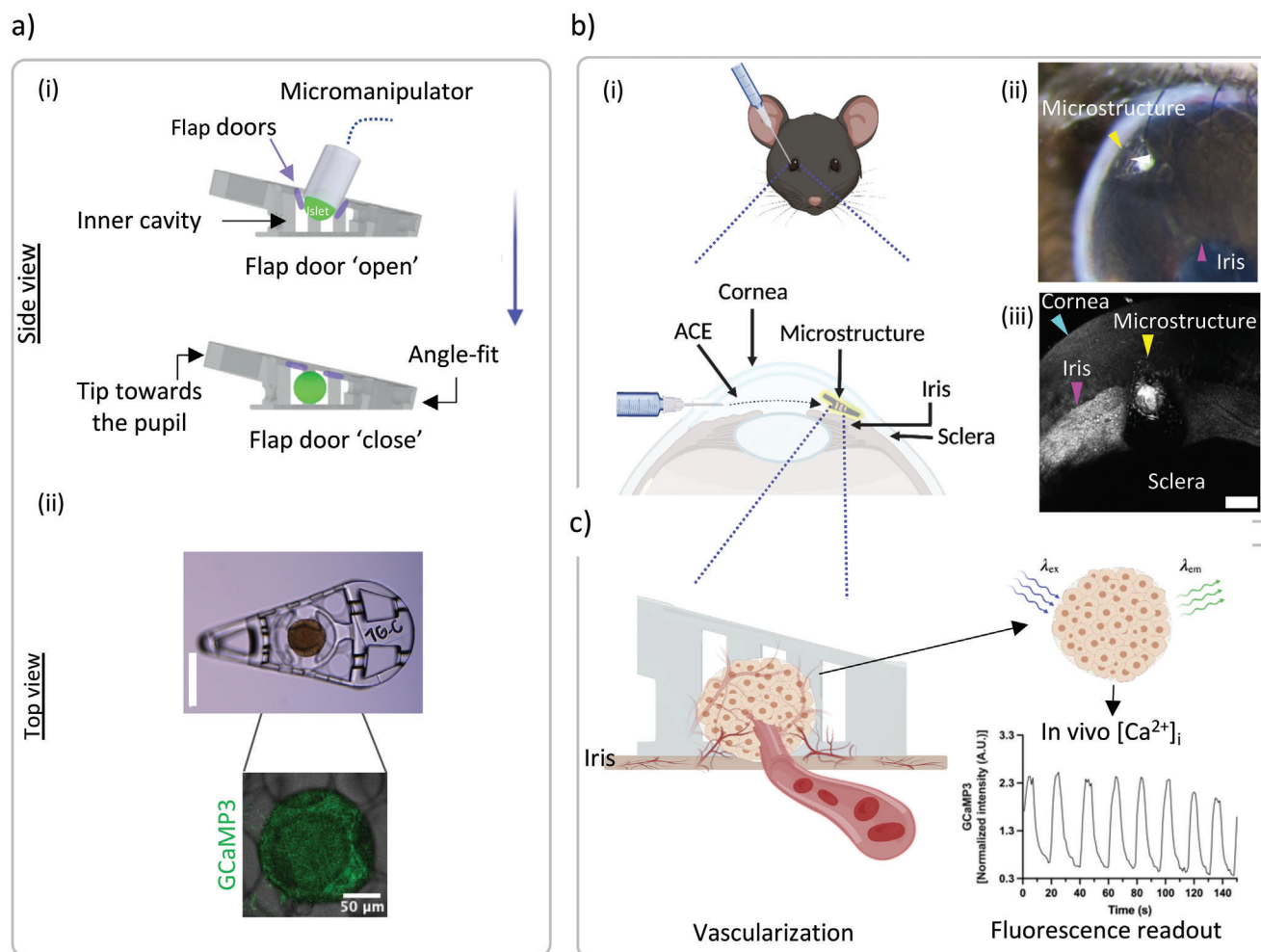


Figure 1. Schematic overview of localization, transplantation, and application of pancreatic islet biohybrid microstructures. a) Microstructures are designed based on the anatomy of the mouse ACE and fabricated via TPP 3D printing. a-i) The microtissue (here pancreatic islet) is placed in the inner cavity of the microstructure using a micromanipulator and mechanically confined by the “flap door” feature that opens during the placement by the gentle pressure of the cannula tip and closes after tip retrieval. a-ii) Photograph of a microstructure with a localized islet inside (Scale bar = 200 μm). The magnified confocal image shows the fluorescence intensity difference between the microstructure and the islet expressing the GCaMP3 biosensor protein. b-i) Sutureless transplantation to the ACE. The microstructure is placed at the iridocorneal angle (located on the circumference of the ACE) through an incision in the cornea. b-ii) Photograph of a mouse eye with a transplanted microstructure. Arrowheads denote the microstructure (yellow), islet (white), and iris (magenta). b-iii) Confocal backscatter image (maximum projection) of a transplanted eye. Corneal transparency allows longitudinal imaging. Arrowheads denote the cornea (cyan), microstructure (yellow), iris (magenta), and sclera (white) (Scale bar = 200 μm). c) Schematic illustration of the engraftment to the host tissue. Ca^{2+} imaging is used to track Ca^{2+} oscillations, as a functional state tracer of the transplants, in vivo.

widespread use in islet transplantation as a curative therapy for type 1 diabetes and their potential for glucose-sensing applications. Several locations are used as islet transplantation sites in rodents and higher mammalian models, including the subcutaneous space, intrahepatic infusion, spleen, kidney capsule, and ACE.^[13] The concept of transplanting tissues within the ACE has been present for over a century.^[14,15] The ACE is an ideal transplantation site due to its immune-privileged status and a high degree of vascularization, which provides an excellent environment for engraftment^[16–19] and allows for tracking host–transplant interactions,^[20–22] studying tissue function (biology/pathology) at single-cell resolution,^[23] and holds significant potential for enhancing preclinical and clinical treatments.^[24,25] While previous studies have engineered hy-

brid scaffolds for subcutaneous islet transplantation^[26–29] and attempts have been made to develop miniaturized sensors to measure IOP directly in the ACE,^[30] no study, to our knowledge, has examined the engraftment of biohybrid microstructures in this location. Nano-/microencapsulation of microtissues in polymer membranes has been widely used although it often creates complexities for metabolite and growth factor diffusion, hinders subsequent engraftment (intra-microtissue vessel development), and is less flexible to be tailored for development of various applications.^[31,32] Our strategy involves assessing engraftment in a micromechanical structure where cells are in direct contact with the ACE microenvironment, allowing for vascular engraftment without altering the structure mechanically.

We aim to investigate the engraftment of biohybrid microstructures (hereafter called microstructures) in the ACE and to provide insights for developing future biohybrid platforms, such as sensors, designed for this site. To successfully integrate biohybrid devices with host biology, three requirements must be met: 1) protection of the microtissue during handling, 2) preservation of functionality of the microtissue, and 3) promotion of integration through vascularization. The coupling of materials to living cells is a coveted topic in biomedical engineering, with potential applications in the localized delivery of therapeutic or immunosuppressive drugs, cell and tissue transplantation, and cell therapy.^[33–36] Furthermore, exploring the unique microenvironment of the ACE as a transplantation site for biohybrid structures is crucial in shaping a general concept in the field.

2. Results and Discussion

2.1. Design and Fabrication of the Microstructure for Microtissue Transplantation in the ACE

To ensure successful sutureless transplantation of microstructures to the mouse ACE, we designed two different microstructures, named “cylinder” and “wedge,” based on the mouse eye’s anatomy^[30] and sutureless transplantation requirements. We used two-photon polymerization (TPP) technique to 3D print these microstructures, as illustrated in Figure S1 (Supporting Information) and Figure 1a. We investigated two different photoresins for the structural component of the microstructures, IP-Visio and IP-S, and ultimately selected IP-Visio due to its suitable optical (such as transparency and autofluorescence) and mechanical properties (Figure S2, Supporting Information). To securely confine the microtissue inside the microstructure during transplantation, we incorporated “flap door” features (Figure S1a, Supporting Information) that open during microtissue placement using a cannula and then mechanically confine the microtissue after placement, as shown in Figure S1b,c (Supporting Information). The flap doors are designed with two flaps, each constructed as a flat surface that tapers at its connection to the main structure. These tapered areas act as inflection points, allowing the flaps to bend when mechanically pressed. The design of the flap door was based on the principle of ensuring compatibility with the size of the islets and also for a seamless mechanism of opening and closing without causing any damaging effects on the microtissue. Furthermore, we accounted for the flap’s ability to return to its original shape without getting stuck inside the microstructure cavity. This design provides a flexible passage for the easy insertion or removal of islets. This feature eliminates the need for additional ECM-like adhesives, such as collagen hydrogels or Matrigel, and avoids related complexities such as tissue/organoid functionality, optical limitations, or diffusion limitation. The cylinder microstructure has a base diameter of 300 μm and height of 240 μm , consisting of a base layer with a diameter of 20 μm macropores for media exchange, a top layer with flap doors for microtissue placement, and seven pillars spaced at 70 μm intervals to connect the base and top layer, as depicted in Figure S1b (Supporting Information).

The wedge is specifically designed to fit and mechanically wedge into the iridocorneal angle of the ACE (Figure 1a) located on the circumference of the ACE, intermediating the sides of the

base of the iris, cornea, sclera, and the anterior surface of the ciliary body.^[37] This location is strategically chosen due to its minimal iris dynamics, which minimizes the risk of continuous displacement during grafting. The rear of the wedge is designed to fit the angle, with the tip oriented toward the pupil. The wedge design also incorporates flap doors for easy placement and mechanical confinement of the microtissue. We incorporated many voids into the cylinder and wedge microstructures to ensure optimal functionality and long-term use. Studies examining pore size (40–632 μm) in different scaffold materials, including beta-tricalcium phosphate, poly(lactic-co-glycolic acid), and polyethylene glycol hydrogels, suggest that large pore sizes generally promote more extensive and sustained vascular ingrowth compared to smaller pore sizes.^[31] Further to their role in promoting vascularization of the confined microtissue, they are necessary to prevent obstruction of aqueous humor drainage via the Schlemm’s canal, which if blocked, could lead to elevated IOP.

2.2. Islet Isolation, Localization in the Microstructure, and In Vitro Functionality

We chose pancreatic islets as our microtissue model and used either wild-type islets or islets that expressed the GCaMP3 Ca^{2+} biosensor in their β -cells (Figure S3a,b, Supporting Information). After islet isolation and a day in culture, we placed the islets inside the microstructures using a cannula and a micromanipulator (Figure 1a). We confirmed islet functionality and absence of mechanical damage by examining their $[\text{Ca}^{2+}]_i$ (cytoplasmic free Ca^{2+} concentration) dynamics in vitro (Figure S3c, Supporting Information), where islets in buffer media containing 11×10^{-3} M glucose presented functional $[\text{Ca}^{2+}]_i$ oscillations. We assessed the in vitro biocompatibility of the IP-Visio photoresin by analyzing the islet glucose stimulation response one week after placement in the microstructure (Figure S3d, Supporting Information). The fluctuations of $[\text{Ca}^{2+}]_i$ in response to different media containing 3×10^{-3} M (basal) and 11×10^{-3} M (high) glucose and 3×10^{-3} M glucose with 25×10^{-3} M KCl, indicated a functional β -cell population (Figure S3d, Supporting Information). KCl promotes β -cell depolarization, leading to a significant influx of Ca^{2+} . Our in vitro results confirmed that the material and localization procedure had no evident adverse effect on β -cell functionality. Previous studies have recorded Ca^{2+} activities in IP-Visio-based platforms designed for nerve growth, differentiation, and co-cultures using Ca^{2+} dyes in vitro.^[38,39] Our results further show that the low background fluorescence intensity of IP-Visio compared to islets expressing GCaMP3 makes it a suitable material combination for evaluating $[\text{Ca}^{2+}]_i$ dynamics.

2.3. Transplantation and Localization in the ACE

We transplanted the microstructures in the ACE of mice using a self-healing cannula placement procedure (detailed in the Experimental Section). This method is a long-standing technique that involves the creation of small incision to facilitate access for transplantation.^[14] We used donor islets 2–4 d after isolation, utilizing the temporary availability of intra-islet donor endothelial cells for elevated revascularization.^[40] Each eye received

one microstructure. As a control, microstructures without islets and bare islets were transplanted. We did not observe any irritation or redness after transplantation and our evaluation spanning over 20 weeks post-transplantation did not unveil any alterations within the ACE or any unusual behavior in mice that might suggest visual impairment.

We initially transplanted seven eyes with cylinder microstructures carrying non-sensor-expressing islets. The size and geometry of the microstructures facilitated the transplantation procedure. We evaluated the mice up to 10 months after transplantation and examined the microstructures for vascularization at several time points (Figure S4, Supporting Information). The eyes showed normal morphology, no visible damage to the cornea was observed from the transplantation procedure, and the insertion incision was healed after a few days. We observed five structures constantly localized on the iris, however their orientation differed at each evaluation time point. We did not detect vascularization in these samples on evaluations after four weeks or ten months post-transplantation (vascular engraftment is detailed in Section 2.6) (Figure S4a,b-i, Supporting Information). In comparison, we observed engraftment in two structures that were physically trapped at the angle during our evaluation four weeks post-transplantation (in contact with the cornea and the iris), and these structures did not show changes in localization or orientation during the experimental period (Figure S4b-ii, Supporting Information).

The low success rate of grafting of the structure on the iris can be linked to the natural iris dynamics.^[41] To resolve this challenge, we designed the wedge microstructure geometry to fit the angle dimensions of the ACE. The intimate surface interaction between the microstructure and the ACE boundary (iris, angle, and cornea) mechanically anchors the microstructure in the ACE. We transplanted 11 wedge microstructures and evaluated them for up to 20 weeks. The wedge dimensions allowed smooth insertion through the incision yet prevented structural movement related to the iris dynamics (Figure 2a). We did not observe wedge rotation or displacement relative to the eye during the experimental period. Although we were successful in minimizing the impact of iris dynamics on the microstructures to a great extent, we could not control the orientation during transplantation, which led to the localization of microstructures in two distinct orientations. Two of them were right-side-up, and nine of them were upside-down (Figure 2b). We found that one wedge-shaped microstructure that was oriented upside-down was not attached or in direct contact with the iris as intended. Instead, it was attached to the cornea, suggesting a misplacement during the transplantation process, possibly due to incorrect placement in the angle. The orientation of wedge microstructures is determined by the initial orientation during transplantation and is not affected by iris dynamics. This suggests that the placement procedure could benefit from additional enhancements. These enhancements may include developing better tools, such as canulas and holders, making modifications to the transplantation procedure, or integrating materials that ensure consistent orientation when transplanted.

Optical coherence tomography (OCT) scans provided confirmation that the cornea remained intact after transplantation (Figure 2c-i) and localization of the microstructures at the terminal time point (Figure 2c-ii). It should be noted that the mi-

crostructure (IP-Visio) is not visible due to its transparency at the acquisition wavelength of the OCT scanner (840 nm). Nevertheless, the islet and the foreign body reaction (FBR) cells attached to the microstructure (detailed in Section 2.5) were visible in the OCT scans.

2.4. In Vivo Functionality

Presence of $[Ca^{2+}]_i$ oscillations after transplantation is a critical indicator of success of the procedure. Our in vivo imaging analysis showed $[Ca^{2+}]_i$ oscillations on the day of transplantation and 2, 8, and 20 weeks after transplantation, as depicted in Figure 2d. Notably, mice were not subjected to fasting to maintain low blood glucose levels or injected with glucose to elevate their blood glucose levels during Ca^{2+} imaging. Therefore, a variation in frequency and magnitude of $[Ca^{2+}]_i$ oscillations on the separate days of recording was expected and observed. Nevertheless, the consistent occurrence of $[Ca^{2+}]_i$ oscillations throughout the study period suggests successful graft integration with the host.

We encountered a challenge in verifying the functionality of the islets in vivo. This was due to the difficulty in imaging objects in the iridocorneal angle, which we found to be the ideal site for microstructure engraftment. The positioning of the microstructure in the angle and the limited field of view caused by the uncontrolled orientation of the microstructure made it challenging to focus on and image the entire islet ($\varnothing \approx 150\text{--}200\ \mu\text{m}$) using confocal imaging. However, despite this limitation, we could record $[Ca^{2+}]_i$ oscillations successfully in 10 out of 11 samples, indicating in vivo functionality of islet β -cells.

2.5. Foreign Body Reaction

Less than 24 h after transplantation in a mouse model recognized for inducing strong FBR,^[29] we observed an accumulation of cells on the microstructure, implying FBR (Figure S4b, Supporting Information). The sparse monolayer coverage of circular cells on the microstructures remained consistent between different in vivo assessment time points, as observed by intravital microscopy.

After graft retrieval at 10 months (cylinder) and 20 weeks (wedge) post-transplantation, we observed that most of the cells covering the microstructure had brownish compartments inside their cytoplasm, indicating the presence of macrophages with phagosomes (Figure 3a). We further investigated the presence of macrophages and foreign body giant cells (FBGCs)^[42] as markers of inflammation on the transplanted structures. We observed cells staining positive for F4/80 (the most specific marker for murine macrophages), CD11b (a marker for murine dendritic cells^[43]), and α -SMA (a myofibroblast marker^[44]) with a round/oval, round/spread, and spindle shape morphology, respectively (Figure 3b,c). We identified multinucleated FBGCs with filopodia^[45] by immunostaining for intracellular vimentin, a highly abundant cytoplasmic intermediate filament protein expressed in inflammatory macrophages (Figure 3d). Since pro- and anti-inflammatory cytokines stimulate macrophages to secrete vimentin,^[46] we also stained the samples for extracellular vimentin (Figure 3e). We found no evidence of thick ECM or accumulation of multilayered cells on the surface of the structure.

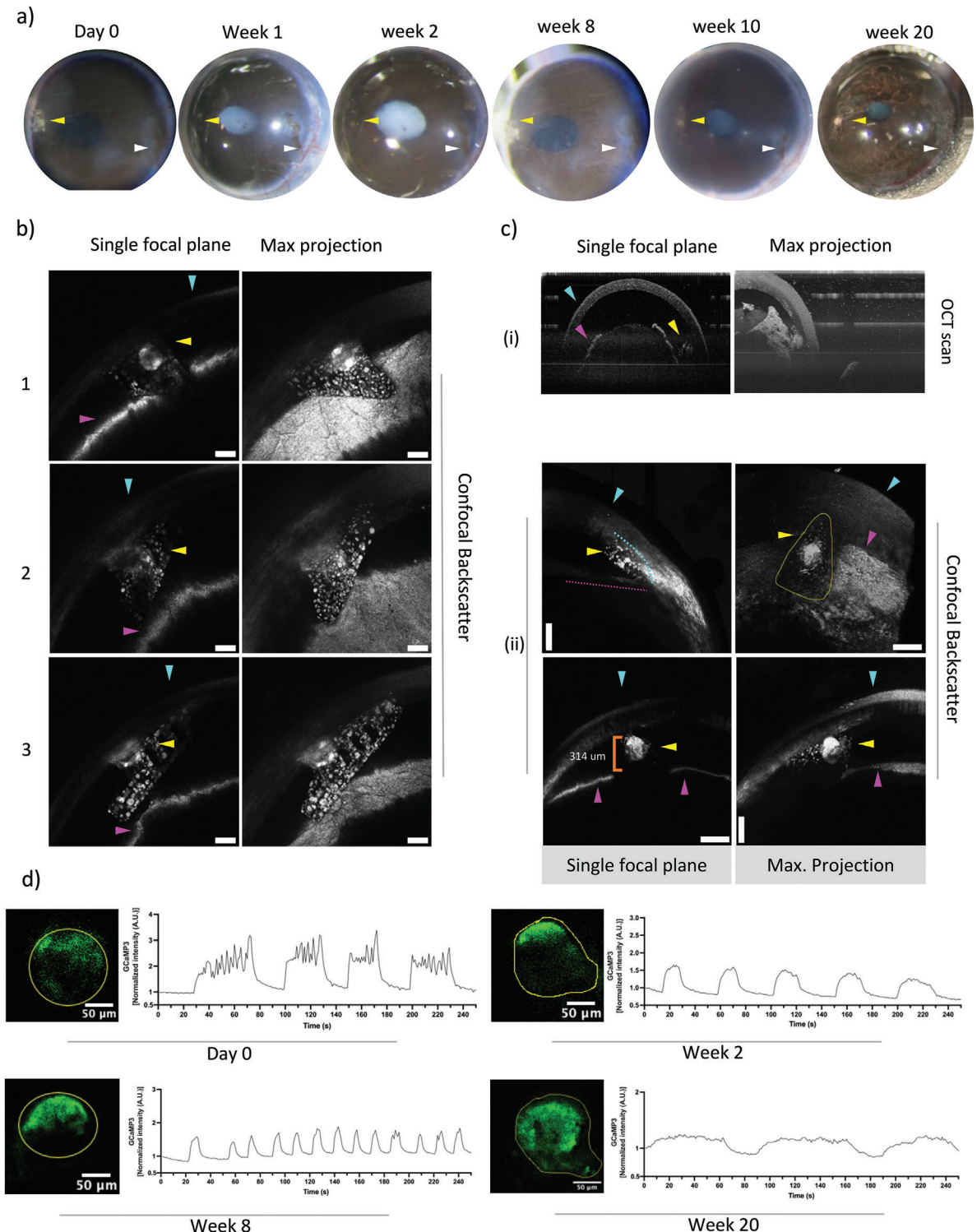


Figure 2. Wedge transplantation and in vivo functionality. a) Photographs of a transplanted eye at different time points show the microstructure firmly localized at the transplantation site. The white arrowhead denotes the transplantation incision and the yellow arrowhead points to the microstructure. The white patches seen in the images of week 1 and week 2 are temporary and frequently observed after the specific anesthesia used. b) Confocal backscatter images from different microstructures (1, 2, and 3 d) after transplantation. Arrowheads denote the cornea (cyan), iris (magenta), and microstructure (yellow) (Scale bar = 100 μm). c-i) OCT scan of an eye transplanted with a microstructure showing intact morphology of the cornea after transplantation. c-ii) Confocal backscatter images of the microstructures at the end of the experiment (Scale bar = 200 μm). Confocal images are presented as maximum intensity projections in the XY-plane. d) Longitudinal intravital $[\text{Ca}^{2+}]_i$ imaging of an islet in a microstructure by confocal microscopy at indicated time points after transplantation. GCaMP3 fluorescence (green) was optically measured and plotted in the respective graphs. Images and graphs represent one sample over the experimental period.

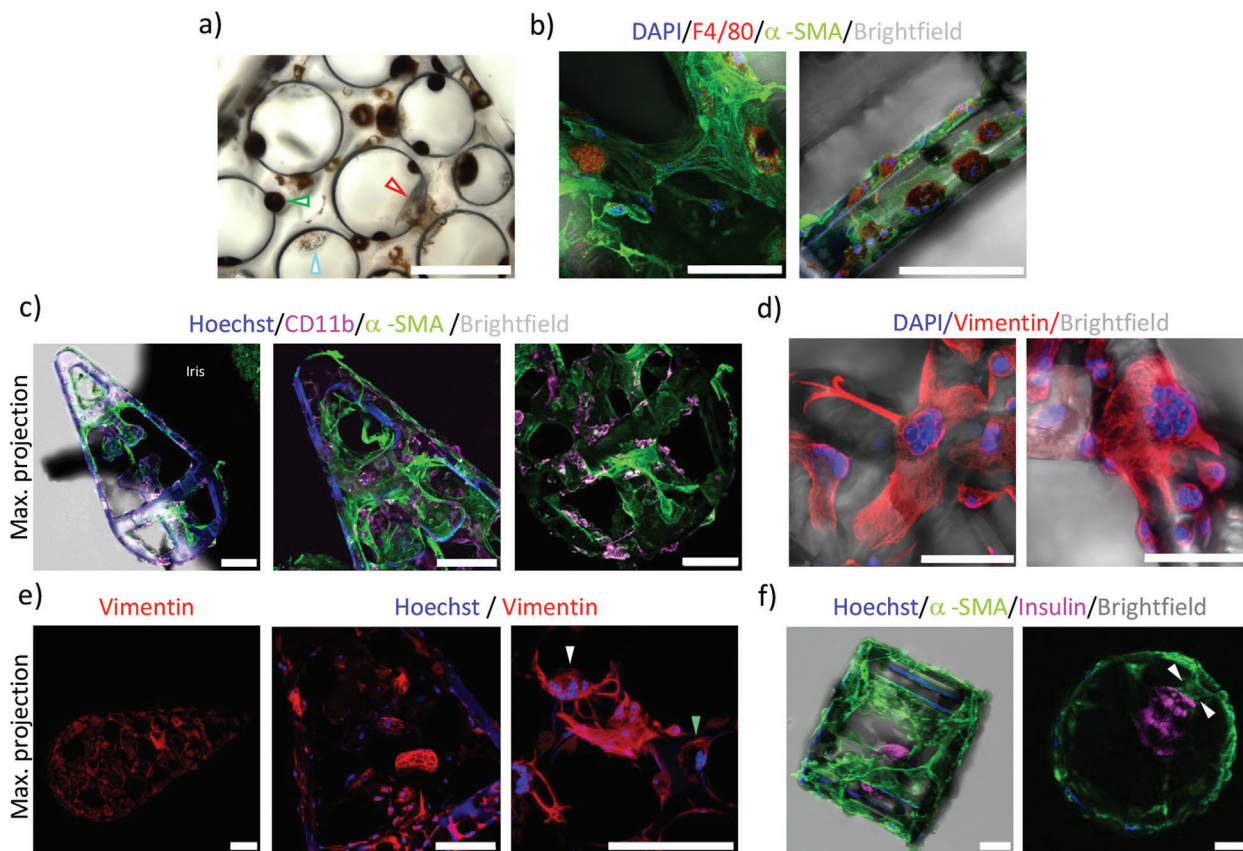


Figure 3. Foreign body reaction characterization of microstructure explants retrieved after 10 months (cylinder) and 20 weeks (wedge) of transplantation. All scale bars represent 100 μm unless otherwise stated. a) Optical image of a microstructure explant covered by cells including a high concentration of phagosome (green arrowhead), moderate cytoplasmic phagosomes (blue arrowhead), and residual endothelial cells (red arrowhead) with noncytoplasmic phagosomes. b,c) Cell characterization by confocal microscopy after immunofluorescently labeling for F4/80, a macrophage marker (red), α -SMA, the myofibroblast marker (green), CD11b, a macrophage marker (magenta), and nuclei (blue). d) Immunofluorescence images of cell cytoskeletal morphology (intermediate filaments) using immunostaining for vimentin (red). Foreign body giant cells (FBGCs) are identified by the appearance of multiple nuclei (Scale bar = 50 μm). e) Immunostaining images of extracellular vimentin secreted by the cells represented in maximum projection. The white arrowhead points to FBGCs, and the green arrowhead points to a cell with incomplete imaging stacks showing the stained cells' cross-sectional view. f) Confocal images of a microstructure (side and top (cross-section) views) with an islet immunolabeled for insulin (magenta) and α -SMA (green). White arrowhead points to the interaction site between the islet and the α -SMA⁺ cells.

This could be attributed to the immune-privileged microenvironment of the ACE or a minimized immunogenicity of IP-Visio. In some samples, we noticed FBR cells partially in contact with the islet (Figure 3f). While studies on intraocular implants such as polyimide micro-stents^[47] transplanted in the supraciliary space and in contact with the aqueous humor have demonstrated fibrosis and other chronic complications, it is suggested that the aqueous humor reinforces fibrotic encapsulation.^[48] Possible direct FBR-islet interaction needs further assessment. However, we did not observe a specific alteration in β -cell function in this study. To our knowledge, this is the first *in vivo* study of IP-Visio and therefore we cannot compare our results with other transplantation studies.

2.6. Vascular Engraftment

The physiological function of pancreatic islets in glycemic control (sensing blood glucose and secreting hormones) requires

vascularization.^[49] Consequently, revascularization of the transplanted islets is a critical step in ensuring their survival and function. To evaluate islet revascularization eight weeks post-transplantation, we injected a fluorescent dye solution into the tail vein of the mouse while monitoring islet fluorescence (Figure 4). We used DyLight conjugated Lectin as the neovascularization tracer to perfuse the vessels. Figure 4a depicts the fluorescent profile of a confined islet within a microstructure before and after injecting the fluorescent dye. Movements related to animal respiration and injection can cause a loss of focus, leading to changes in signal (Figure 4a-iii). As a positive control for observing engraftment, we also transplanted bare islets, for which vascularization is stimulated by the proximity to the abundant vessels in the iris (Figure 4b). Previous studies conducted in dorsal skin,^[49] kidney capsule,^[40] and the ACE,^[50] have shown that capillary sprouts and new vessels start to form in transplanted islets within 2–4 d after transplantation.

During *in vivo* imaging, we observed the perfusion of ten confined islets with the fluorescent dye, confirming successful

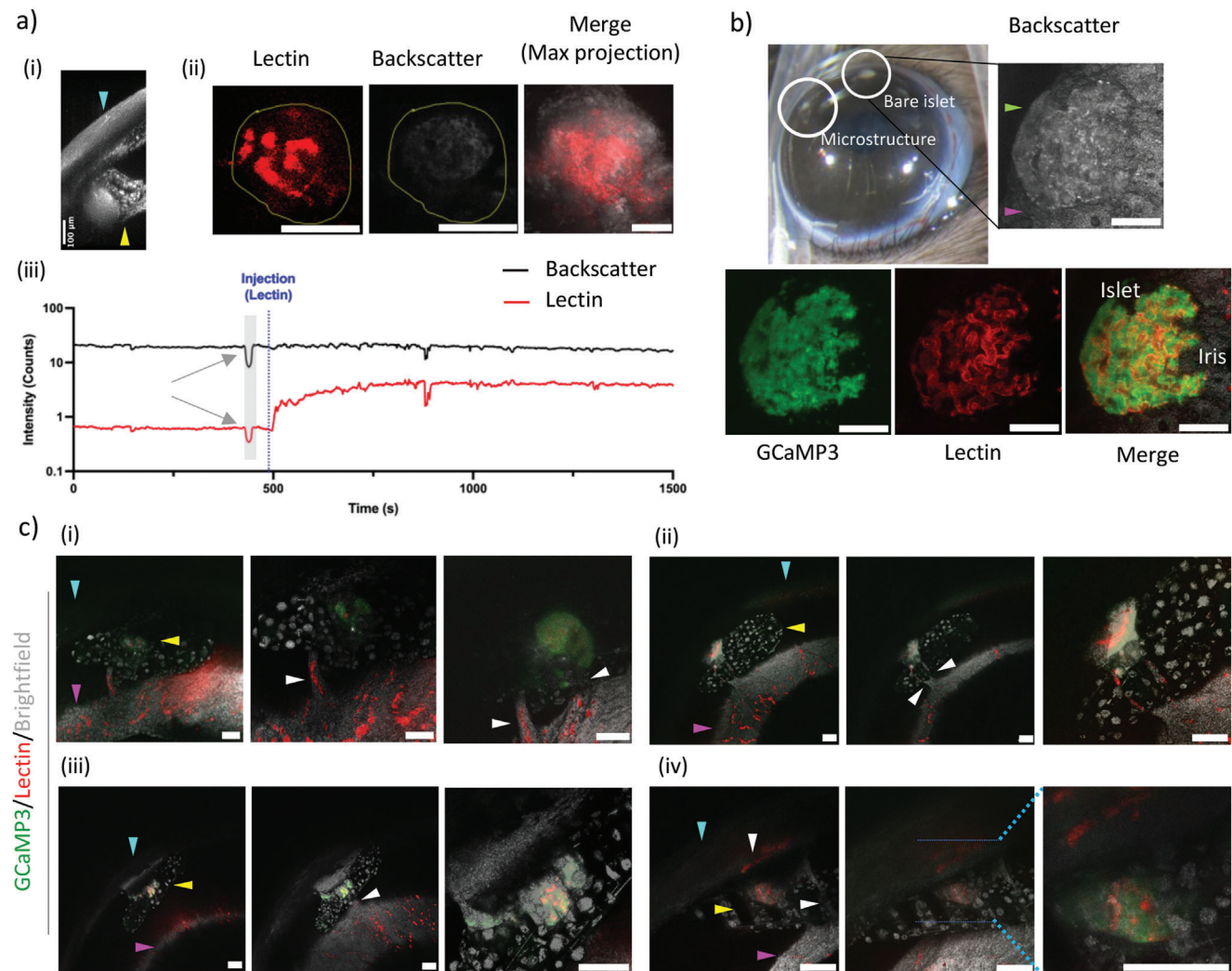


Figure 4. Biohybrid microstructure vascularization. All scale bars represent 100 μm unless otherwise stated. Arrowheads denote cornea (cyan), microstructure (yellow), iris (magenta), and vessels (white). a-i) Confocal backscatter image of a transplanted microstructure. a-ii) Intravital fluorescence image of a microstructure 20 weeks after transplantation. The fluorescent dye, DyLight-Lectin, perfused blood vessels and was administered through tail vein injection (Scale bar = 50 μm). The time-dependent increase in fluorescence signal plotted in (a-iii) indicates successful vascularization of the islet. The arrows point to the animal's transient movement (motion artifact) during preparation for injection, while the dotted line marks the time when the dye reaches the intra-islet vessels via the bloodstream. Movements result in a loss of focus and changes in the signal that could also be seen in the backscatter/reflection channel. b) Photograph of an eye transplanted with a microstructure and a bare islet as a positive control for the engraftment procedure. Confocal images of the engrafted bare islet to the iris with the β -cells expressing GCaMP3 (green) and vessels perfused with DyLight-Lectin (red). Green arrowhead points to the islet grafted to the iris (magenta arrowhead). c) Intravital fluorescence imaging of transplanted microstructures. c-i) Image of an islet being vascularized from the iris. c-ii) Vessels (white arrowheads) from the iris have sprouted and branched to vascularize the islet despite being far and in no direct contact (in a few tens of micrometers away) with the iris. A fully vascularized islet is also shown in (c-iii), which has been vascularized from the iris. Although most samples are vascularized from the iris, (c-iv) shows a sample that is vascularized from both the iris and the cornea.

engraftment. We observed that seven of these islets were vascularized from the iris, with the vascular connections originating from beneath the islets as well as from the surrounding region in close proximity (Figure 4c-i–iii). Notably, we observed that there were vascular connections to the iris in the microstructure that was not in direct contact with the iris (Figure 4c-ii). This microstructure was only secured mechanically to the cornea, and upon dissecting the eye and breaking the delicate free-standing vasculature, we found that the microstructure was entirely free-floating.

Vascular network formation is an intricate process that involves endothelial cells, soluble growth factors, extracellular matrix (ECM) components as well as remodeling and is influenced by biochemical and biomechanical cues in the microenvironment.^[51,52] Our results present compelling evidence of endothelial sprouting through the ECM-free microenvironment of aqueous humor. The aqueous humor is secreted at a rate of 1.5–3.0 $\mu\text{L min}^{-1}$ and undergoes clearance approximately every 100 min,^[53,54] resulting in a complex signaling

environment for pro-angiogenic mediators such as vascular endothelial growth factor (VEGF).

In the three remaining samples, we observed that the islets had vascular connections to the iris and cornea, as shown in Figure 4c-iv, representing a typical sample with a good transplantation procedure and a fully localized islet in the microstructure. However, in the second sample, a mechanical complication during transplantation led to cornea damage, resulting in subsequent haziness of the cornea, as shown in Figure S5a (Supporting Information). This haziness suggested a condition known as cornea edema, which can occur when the cornea becomes excessively hydrated and gradually loses transparency, leading to corneal vascularization.^[55] Cornea edema can arise from various causes, including surgical interventions. For instance, a study^[56] reported that a retained lens fragment, measuring $960\ \mu\text{m} \times 750\ \mu\text{m}$, after phacoemulsification in the ACE, caused cornea edema. Finally, in one of the 11 cases, the islet was trapped between the flap doors. Fifteen weeks after transplantation, we observed the islet outside the microstructure and attached to the cornea, exhibiting morphological changes (Figure S5b-i, Supporting Information). Furthermore, we observed that the islet had a vascular connection with the iris and cornea, as shown in Figure S5b-ii (Supporting Information). In this sample, we observed the same vascular extensions in the aqueous humor as in the previous samples that had solely vascular connection with the iris. In this sample, we recorded $[\text{Ca}^{2+}]_i$ oscillation at week 15 post-transplantation.

Graft revascularization rates depend on various factors such as blood vessel density of the transplanted site, inflammation, oxygen tension, and intra-islet endothelial cells.^[51,52,57] Our approach did not involve using exogenous angiogenic growth factors, such as VEGF, to induce or accelerate vascular engraftment. The entire engraftment process relied on the inherent physiological interactions between the microtissue (transplanted islets secrete VEGF) and the ACE microenvironment. In addition, the VEGF produced by FBGCs helps recruit and maintains immature neovessel.^[58] It has also been proposed that extracellular vimentin secreted by FBGCs is pro-angiogenic and has similar functionality as VEGF, including VEGF-receptor signaling.^[59] In the context of biohybrid engraftment, the role of FBR in forming and maintaining the vascular network can be advantageous. Further investigation is necessary to determine the exact role of FBR in biohybrid engraftment and to potentially modulate FBR for more favorable engraftment outcomes.

3. Conclusion

In this study, we focused on investigating biohybrid microstructure transplantation. We used TPP's benefits to fabricate microstructures capable of delivering and fixating microtissues in the ACE. The fabrication procedure is simple and easily adjustable to fit various tissues. The flap door feature makes microtissue confinement free from using additional adhesive materials, such as hydrogels. This strategy can be used for various applications such as biohybrid sensors, microtissue delivery, and defined tissue–tissue interaction studies. We report the first transplantation and in vivo study on IP-Visio, as an off-the-shelf material. We provide evidence that the material is biocompatible with pancreatic islets by evaluating their in vitro/in vivo func-

tionality and observed minimal signs of FBR upon transplantation. We show that the corneal transparency and tissue morphology remain unaffected after transplantation and 20 weeks post-transplantation. However, more research is necessary to understand the material's immunogenicity in other tissue microenvironments. This could involve exploring different surface modification or coating approaches, such as local delivery of anti-inflammatory or antifibrotic agents,^[60] to promote subsequent tissue repair and improve the biohybrid transplant's functionality.

We used pancreatic islets expressing a genetically encoded Ca^{2+} indicator (GEC1), GCaMP3, to evaluate their in vivo functionality over the transplantation period. GECIs are ideal for evaluating cell function in transplantable biohybrid devices since they enable longitudinal readouts and avoid the challenges associated with using fluorescent dyes in vivo, such as labeling and injection, concentration optimization, and experimental repeatability due to their short half-life.^[61] After evaluating the in vitro functionality of the microstructures, we assessed the in vivo functionality and vascularization over 20 weeks using microscopy. Our analysis of different microstructures suggests that the dynamics of the iris is a critical factor for successful engraftment and, in this context, the localization and stability of the transplanted microstructures are essential. By targeting the iridocorneal angle, where the iris dynamics are minimal, we developed a more stable geometry for our microstructure design. The difficulty in imaging and verifying the functionality of the transplanted microstructures in the angle highlights the need for further improvements in the sensing modules. One promising solution is the development of integrated biohybrid sensors that can provide real-time monitoring of microtissue function. Such sensors could potentially overcome limitations of current imaging techniques and provide more accurate data on the functionality of biological units.

Our work represents a significant advance in the field of biohybrid structural engraftment in the ACE, providing compelling empirical evidence of successful integration. Moreover, our study highlights the potential for this unique site and strategy to be leveraged in a broad range of investigations requiring bio-microsystem integration with the host microenvironment. This includes studies enabling real-time measurements of physiological responses with high specificity and sensitivity, investigations into various microtissue–microtissue interactions, and exploration of ECM-free vascularization strategies. Our finding that endothelial sprouting can occur in a dynamic fluid environment with low viscosity underscores the critical role that the physical and chemical properties of the microenvironment play in tissue regeneration and integration. By shedding light on these fundamental principles, our work lays a foundation for future research to improve the efficacy of biohybrid structural integration and tissue engineering strategies.

4. Experimental Section

Mice for Isolation and Transplantation: The sensor expressing islet, expressing the fluorescent Ca^{2+} indicator protein (GCaMP3), was obtained from heterozygous donor mice (RIP-Cre;GcaMP3).^[23] The recipient mice, immunocompetent C57BL/6j, were obtained from the breeding colony

at Karolinska Institutet, Stockholm, Sweden. Mice were kept on a 12 h light/12 h dark cycle. All experimental procedures and animal studies were carried out in strict accordance with the Karolinska Institutet's guidelines for the care and use of animals in research and were approved by the regional Animal Ethics Committee (No. 1184-2021).

Islets of Langerhans Isolation and Culture: Pancreatic islets were isolated from 8 to 10 weeks old adult wild-type and double heterozygous RIP-Cre:GCaMP3 male mice. In brief, mice were sacrificed by cervical dislocation and incision was made in the abdominal region to gain access to the internal cavity. To ensure controlled containment, the common bile duct was methodically clamped, limiting the spread of the digestion buffer in pancreas after bile duct injection. The digestion buffer consisted of ice-cold collagenase P (1.5 mg mL⁻¹, Roche) in the washing buffer (Hanks' Balanced Salt Solution (HBSS, Gibco) supplemented with BSA (2.5 mg mL⁻¹, Fisher) in HEPES (25 × 10⁻³ M, Gibco), and pH adjusted to 7.4). The perfused pancreas was separated from the abdomen, collected in a vial containing the washing buffer, and placed in a water bath (37 °C, 25 min). To help with liberation from the tissue ECM, the digested solution was passed through an 18G steel needle and washed (twice, 5 min). Islets were handpicked under a stereomicroscope and incubated at standard conditions (37 °C, 5% CO₂, in humidified air) in a medium containing RPMI-1640 (Gibco) supplemented with 10% FBS (Gibco), L-Glutamine (2 × 10⁻³ M, Gibco), penicillin (100 IU mL⁻¹, Gibco), and streptomycin (100 µg mL⁻¹, Gibco) until use.

Microstructure Fabrication and Islet Localization: Microstructures were fabricated in a single printing procedure using a commercial TPP 3D printer (Nanoscribe) in a commercially available biocompatible photoresin (IP-Visio and IP-S, Nanoscribe). According to the MSDS of the supplier, IP-Visio photoresin is composed of (95%) 7,7,9(or 7,9,9)-trimethyl-4,13-dioxo-3,14-dioxo-5,12-diazahexadecane-1,16-diylobismethacrylate, (<1%) phenylbis(2,4,6-trimethylbenzoyl)phosphine oxide, (<2%) (bis(2-methacryloxyethyl)-N,N'-1,9-nonylenebiscarbamate), and (<1%) 2,6-di-*tert*-4-butylhydroxytoluene. Photoresin was dispensed on indium tin oxide (ITO) coated glass, and the designs (designed in SolidWorks) were printed. Following TPP structuring, samples were developed in propylene glycol methyl ether acetate (PGMEA, Sigma-Aldrich) and washed with isopropanol (VWR Chemicals) for 25 and 5 min, respectively. To prepare the structure for hosting an islet inside, samples were washed with culture media and centrifuged (2200 g for 5 min) to remove air bubbles trapped inside the microstructure voids. Islets were picked and localized in the structures using a micromanipulator (Eppendorf, 5170). Borosilicate glass micropipettes were pulled and grinded to create microcapillaries or cannulas. Islets were localized inside the microstructures 1 d after isolation. This delay gave the freshly isolated islets time to produce ECM around themselves and better tolerate the possible mechanical tensions during the localization procedure.

In Vitro [Ca²⁺]_i Imaging: Four samples consisting of a wild-type islet, biosensor (GCaMP3) expressing islet, microstructure made of IP-S, and IP-Visio were prepared. Their fluorescence was examined using a laser scanning confocal microscope (TCS SP8, Leica) with gating of the emission signal to exclude reflection. To check the functionality of the localized islets before transplantation and absence of mechanical damage stemming from the localization procedure, in vitro confocal Ca²⁺ imaging was acquired. To verify the biocompatibility of IP-Visio on islet's function, samples were localized in the structures, and a stimulation experiment, using 3 or 11 × 10⁻³ M glucose, and KCl (25 × 10⁻³ M), was performed after one week of culture using wide-field Ca²⁺ imaging as previously described.^[23] Microstructures were first incubated in low glucose buffer medium (3 × 10⁻³ M) for 1 h, and after 100 s of baseline Ca²⁺ signal recording, media was changed to a higher glucose concentration (11 × 10⁻³ M) and then back to a low glucose medium. In the final step, KCl was added to depolarize the cells. The experiment was conducted at 37 °C.

Transplantation: Microstructures were manually transplanted in the ACE of 8–10 weeks old C57BL/6J mice. Mice were anesthetized with isoflurane (2%–2.5% (v/v), Baxter) using the UNIVENTOR 400 anesthesia unit, and the head was supported and fixed under a stereomicroscope using a head holder (Narishige). Body temperature was maintained at 37 °C ± 0.5 using a heating pad. A small incision was manually created on the cornea

near the sclera using an 18-gauge steel needle. The microstructure was carefully transplanted in the ACE using a glass capillary connected to a Hamilton syringe via polyethylene tubing. Microstructures were injected in the ACE and positioned on the iris and at the iridocorneal angle. A drop of Viscotears (Novartis) was placed on the cornea to avoid desiccation. To visualize the state of the cornea after transplantation regarding any damage created during transplantation, eyes were visualized using an OCT scanner (OQ LabScope, Lumedica).

In Vivo [Ca²⁺]_i Imaging of the Transplanted Islets: Anesthesia was induced and maintained by inhalation of vaporized isoflurane. Mice were fixed with the head holder and placed on the customized confocal laser scanning microscope (TCS SP5, Leica) stage as previously described.^[62] Viscotears was used as an immersion medium between the eye and the objective. Fluorescence emission from GCaMP3 was acquired at λ_{exc} = 488 nm and λ_{emi} = 500–550 nm. To visualize the microstructure and its location in the ACE, a backscatter signal was also acquired by a 633 nm laser (λ_{exc}: 633 nm, λ_{emi}: 630–636 nm). In vivo Ca²⁺ imaging was performed on the day of transplantation and after 1, 2, 8, and 20 weeks post-transplantation.

In Vivo Vascularization Assessment: For in vivo vascularization, perfused blood vessels were identified by intravenous injection of DyLight 649 conjugated Lectin (1 mg per mouse, Invitrogen) using microscopy.

Immunohistochemistry: Animals were euthanized by cervical dislocation, and eyes were enucleated and fixed immediately (2 h) in formalin solution (10% neutral buffered, Sigma). Microstructures were then retrieved from the ACE and permeabilized and blocked using a buffer (0.25% Triton X100 (Sigma-Aldrich) and 10% FBS in 1× PBS). Samples stained for extracellular vimentin were not permeabilized and the buffer excluded Triton-X100. Samples were then incubated (overnight at 4 °C) with a cocktail of primary antibodies diluted in a buffer (0.25% Triton-X100 and 5% FBS in 1× PBS). The primary antibodies used in this study include anti-vimentin (Abcam ab92547, 1:100), anti-α-smooth muscle actin (α-SMA) (Invitrogen, 1:500), anti-F4/80 (Invitrogen, 1:100), anti-CD11b (BD Bioscience, 1:200), and anti-insulin (Dako 1:200). Samples were washed three times in blocking buffer and incubated with the secondary antibodies (1–2 h, room temperature). After three additional washes with PBS, nuclei were stained using DAPI (1:1000) or Hoechst (1:2000) and visualized using a laser scanning confocal microscope.

Supporting Information

Supporting Information is available from the Wiley Online Library or from the author.

Acknowledgements

This work was supported by the Swedish Foundation for Strategic Research (SSF Grant Project No. RMX18-0066). P.-O.B. acknowledges funding support from Berth von Kantzow's Foundation, the European Research Council (Grant No. ERC-2018-AdG 834 860 EYELETS), the Family Erling-Persson Foundation, Funds at Karolinska Institutet, the Jonas & Christina af Jochnick Foundation, the Swedish Diabetes Association, the Swedish Research Council, and the Novo Nordisk Foundation. H.K. acknowledges funding from the Wenner-Gren foundation (UPD2021-0185). A.H. acknowledges funding from Knut and Alice Wallenberg Stiftelse (2020.0206). A.H.'s work was supported by Aimes – Center for the Advancement of Integrated Medical and Engineering Sciences (www.imes.se), Karolinska Institutet (1-249/2019), KTH Royal Institute of Technology (VF-2019-0110) and Getinge AB (4-1599/2018). The authors would like to thank the SSF project partners and their team members for close collaboration and valuable discussions, including Prof. Göran Stemme, Assoc. Prof. Niclas Roxhed (KTH Royal Institute of Technology, Sweden), and Prof. Atila Alvandpour (Linköping University, Sweden). The authors would also like to thank the members of the Berggren group specially Dr. Ismael Valladolid Acebes and Dr. Noah Moruzzi (The Rolf Luft Research Center for Diabetes and Endocrinology, Karolinska Institutet, Sweden) and Prof. Helder André (St. Erik Eye Hospital, Karolinska Institutet, Sweden) for helpful discussions.

Conflict of Interest

P.-O.B. is the founder and CEO of Biocrine, a small biotech company that uses the ACE as a screening tool, and M.K. is a consultant for the same company.

Author Contributions

H.K. and M.V. contributed equally to this work. H.K. designed the study, designed and prepared the biohybrid microstructures, collected data, analyzed data, and wrote the original draft. M.V. performed the in vivo experiments, collected data, analyzed data, and edited the paper. M.K. designed the study, collected data, analyzed data, and edited the manuscript. W.W. designed the study, supervised the development of structural design and fabrication methods, analyzed data, and revised and edited the paper. P.-O.B. conceived the original idea, supervised the establishment of all biological evaluations, and revised the paper. A.H. designed the study, supervised the development of material, design, and integration methods, analyzed data, revised and edited the paper. W.W., P.-O.B., and A.H. are all corresponding authors and equal contributors with respect to their specific areas. All authors approved the final version of the paper.

Data Availability Statement

The data that support the findings of this study are available from the corresponding author upon reasonable request.

Keywords

anterior chamber of the eye, biohybrid, microstructures, microtissues, pancreatic islets, vascularization

Received: July 8, 2023

Revised: September 14, 2023

Published online:

- [1] R. Herbert, H.-R. Lim, B. Rigo, W.-H. Yeo, *Sci. Adv.* **2022**, *8*, eabm1175.
- [2] Q. Chen, H. Xie, L. Xi, J. *Biophotonics* **2019**, *12*, 201900066.
- [3] D.-W. Park, J. P. Ness, S. K. Brodnick, C. Esquibel, J. Novello, F. Atry, D.-H. Baek, H. Kim, J. Bong, K. I. Swanson, A. J. Suminski, K. J. Otto, R. Pashaie, J. C. Williams, Z. Ma, *ACS Nano* **2018**, *12*, 148.
- [4] D. Bien, M. Michalczyk, D. Szkopek, M. Kinsner, P. Konieczka, *Sci. Rep.* **2022**, *12*, 13817.
- [5] J. Kim, J. Kim, M. Ku, E. Cha, S. Ju, W. Y. Park, K. H. Kim, D. W. Kim, P.-O. Berggren, J.-U. Park, *Nano Lett.* **2019**, *20*, 1517.
- [6] C. Wang, Z. Zhang, J. Wang, Q. Wang, L. Shang, *Mater. Today Bio* **2022**, *16*, 100352.
- [7] S. Neta, G. Ariel, Y. Yossi, A. Amir, M. M. Ben, *Biosens. Bioelectron.* **2023**, *221*, 114919.
- [8] C. Qin, C. Chen, Q. Yuan, N. Jiang, M. Liu, Y. Duan, H. Wan, R. Li, L. Zhuang, P. Wang, *Anal. Chem.* **2022**, *94*, 6976.
- [9] H. Oda, K. Kihara, Y. Morimoto, S. Takeuchi, *Cyborg Bionic Syst.* **2021**, *2021*, 8907148.
- [10] J. Yang, L. Zu, G. Li, C. Zhang, Z. Ge, W. Wang, X. Wang, B. Liu, N. Xi, L. Liu, *Acta Biomater.* **2023**, *158*, 747.
- [11] T. Ha, S. Park, M. Shin, J.-Y. Lee, J.-H. Choi, J.-W. Choi, *Chem. Eng. J.* **2023**, *463*, 142284.
- [12] U. Yong, D. Kim, H. Kim, D. G. Hwang, S. Cho, H. Nam, S. Kim, T. Y. Kim, U. Jeong, K. Kim, *Adv. Mater.* **2022**, *35*, 2208983.
- [13] F. Cayabyab, L. R. Nih, E. Yoshihara, *Front. Endocrinol.* **2021**, *12*, 1077.
- [14] J. C. Dooremaal, *Albrecht von Graefes Arch. Ophthalmol.* **1873**, *19*, 359.
- [15] R. E. Coupland, *J. Endocrinol.* **1960**, *20*, 69.
- [16] P. Medawar, *Br. J. Exp. Pathol.* **1948**, *29*, 58.
- [17] E. Ilegems, P.-O. Berggren, *Front. Endocrinol.* **2021**, *12*, 652853.
- [18] M. R. Urist, F. C. Mclean, *J. Bone Jt. Surg., Am. Vol.* **1952**, *34*, 443.
- [19] L. Olson, K. Seiger, *Z. Zellforsch. Mikrosk. Anat.* **1972**, *135*, 175.
- [20] S. Speier, D. Nyqvist, O. Cabrera, J. Yu, R. D. Molano, A. Pileggi, T. Moede, M. Köhler, J. Wilbertz, B. Leibiger, *Nat. Med.* **2008**, *14*, 574.
- [21] S. Speier, D. Nyqvist, M. Köhler, A. Caicedo, I. B. Leibiger, P.-O. Berggren, *Nat. Protoc.* **2008**, *3*, 1278.
- [22] E. Ilegems, A. Dicker, S. Speier, A. Sharma, A. Bahow, P. K. Edlund, I. B. Leibiger, P.-O. Berggren, *Proc. Natl. Acad. Sci. USA* **2013**, *110*, 20581.
- [23] S. Jacob, M. Köhler, P. Tröster, M. Visa, C. F. García-Prieto, T. Alanentalo, T. Moede, B. Leibiger, I. B. Leibiger, P. Berggren, *FASEB J.* **2020**, *34*, 945.
- [24] K. Ávall, Y. Ali, I. B. Leibiger, B. Leibiger, T. Moede, M. Paschen, A. Dicker, E. Daré, M. Köhler, E. Ilegems, *Proc. Natl. Acad. Sci. USA* **2015**, *112*, E2611.
- [25] S. B. B. Tun, M. Chua, R. Hasan, M. Köhler, X. Zheng, Y. Ali, M. H. Abdulreda, L. Juntti-Berggren, V. A. Barathi, P.-O. Berggren, *Cell Transplant.* **2020**, *29*, 096368972091325.
- [26] A. R. Mridha, T. R. Dargaville, P. D. Dalton, L. Carroll, M. B. Morris, V. Vaithilingam, B. E. Tuch, *Tissue Eng., Part A* **2022**, *28*, 212.
- [27] C. B. Ahn, J.-H. Lee, J. H. Kim, T. H. Kim, H.-S. Jun, K. H. Son, J. W. Lee, *Bio-Des. Manuf.* **2022**, *5*, 265.
- [28] X. Liu, S. D. Carter, M. J. Renes, J. Kim, D. M. Rojas-Canales, D. Penko, C. Angus, S. Beirne, C. J. Drogemuller, Z. Yue, *Adv. Healthcare Mater.* **2019**, *8*, 1801181.
- [29] O. Veiseh, J. C. Doloff, M. Ma, A. J. Vegas, H. H. Tam, A. R. Bader, J. Li, E. Langan, J. Wyckoff, W. S. Loo, S. Jhunjunwala, A. Chiu, S. Siebert, K. Tang, J. Hollister-Lock, S. Aresta-Dasilva, M. Bochenek, J. Mendoza-Elias, Y. Wang, M. Qi, D. M. Lavin, M. Chen, N. Dholakia, R. Thakrar, I. Lacić, G. C. Weir, J. Oberholzer, D. L. Greiner, R. Langer, D. G. Anderson, *Nat. Mater.* **2015**, *14*, 643.
- [30] D. Ha, W. N. De Vries, S. W. M. John, P. P. Irazoqui, W. J. Chappell, *Biomed. Microdevices* **2012**, *14*, 207.
- [31] X. Ma, S. Dewan, J. Liu, M. Tang, K. L. Miller, C. Yu, N. Lawrence, A. D. McCulloch, S. Chen, *Acta Biomater.* **2019**, *95*, 319.
- [32] R. P. Accolla, A. M. Simmons, C. L. Stabler, *Adv. Healthcare Mater.* **2022**, *11*, 2200243.
- [33] N. Ueda, S. Sawada, F. Yuasa, K. Kato, K. Nagahama, *ACS Appl. Mater. Interfaces* **2022**, *14*, 52618.
- [34] L. R. Doblado, C. Martínez-Ramos, J. M. García-Verdugo, V. Moreno-Manzano, M. M. Pradas, *J. Neural Eng.* **2021**, *18*, 0460c5.
- [35] V. Y. Prinz, K. B. Fritzler, *Adv. Mater. Technol.* **2022**, *8*, 2101633.
- [36] J. M. Gammon, S. T. Carey, V. Saxena, H. B. Eppler, S. J. Tsai, C. Paluskiewicz, Y. Xiong, L. Li, M. Ackun-Farmmer, L. H. Tostanoski, E. A. Gosselin, A. A. Yanes, X. Zeng, R. S. Oakes, J. S. Bromberg, C. M. Jewell, *Nat. Commun.* **2023**, *14*, 681.
- [37] R. Koprowski, Z. Wróbel, S. Wilczyński, et al., *Biomed. Eng. Online* **2013**, *12*, 40.
- [38] Z. Wei, T. Sun, S. Shimoda, Z. Chen, X. Chen, H. Wang, Q. Huang, T. Fukuda, Q. Shi, *Lab Chip* **2022**, *22*, 1006.
- [39] S. Buchmann, A. Enrico, M. A. Holzreuter, M. Reid, E. Zeglio, F. Niklaus, G. Stemme, A. Herland, *Mater Today Bio* **2023**, *21*, 100706.
- [40] D. Nyqvist, S. Speier, R. Rodriguez-Diaz, R. D. Molano, S. Lipovsek, M. Rupnik, A. Dicker, E. Ilegems, E. Zahr-Akrawi, *J. Molina Diabetes* **2011**, *60*, 2571.
- [41] J. Reimer, M. J. Mcginley, Y. Liu, C. Rodenkirch, Q. Wang, D. A. Mccormick, A. S. Toliás, *Nat. Commun.* **2016**, *7*, 13289.
- [42] N. Noskovicova, B. Hinz, P. Pakshir, *Cells* **2021**, *10*, 1794.
- [43] K. M. Adusei, T. B. Ngo, K. Sadtler, *Acta Biomater.* **2021**, *133*, 17.

- [44] D. Zhang, Q. Chen, C. Shi, M. Chen, K. Ma, J. Wan, R. Liu, *Adv. Funct. Mater.* **2021**, *31*, 2007226.
- [45] Z. Sheikh, P. J. Brooks, O. Barzilay, N. Fine, M. Glogauer, *Materials* **2015**, *8*, 5671.
- [46] N. Mor-Vaknin, A. Punturieri, K. Sitwala, D. M. Markovitz, *Nat. Cell Biol.* **2003**, *5*, 59.
- [47] K. J. Habbe, M. Kohlhaas, C. Langwieder, S. Fili, *Clin. Exp. Ophthalmol.* **2023**, *261*, 513.
- [48] K. I. Jung, S.-B. Lee, J. H. Kim, C. K. Park, *Invest. Ophthalmol. Visual Sci.* **2013**, *54*, 3957.
- [49] M. Brissova, A. Shostak, M. Shiota, P. O. Wiebe, G. Poffenberger, J. Kantz, Z. Chen, C. Carr, W. G. Jerome, J. Chen, *Diabetes* **2006**, *55*, 2974.
- [50] I. B. Leibiger, P.-O. Berggren, *Mol. Metab.* **2017**, *6*, 1002.
- [51] Y. B. Li, C. Sodja, M. Rukhlova, J. Nhan, J. J. A. Poole, H. Allen, S. Yimer, E. Baumann, E. Bedford, H. Prazak, *Int. J. Bioprint.* **2023**, *30*, e00258.
- [52] C.-W. Chang, H.-C. Shih, M. G. Cortes-Medina, P. E. Beshay, A. Avendano, A. J. Seibel, W.-H. Liao, Y.-C. Tung, J. W. Song, *ACS Appl. Mater. Interfaces* **2023**, *15*, 15047.
- [53] W. Wang, X. Qian, H. Song, M. Zhang, Z. Liu, *Biomed. Eng. Online* **2016**, *15*, 569.
- [54] D. K. Sunderland, A. Sapra, *StatPearls [Internet]* **2022**, 31985990.
- [55] Q. Akolawala, M. Rovituro, H. H. Versteeg, A. M. R. Rondon, A. Accardo, *ACS Appl. Mater. Interfaces* **2022**, *14*, 20778.
- [56] A. Vasavada, R. Pandit, V. Nath, S. Vasavada, V. Vasavada, *Am. J. Ophthalmol. Case Rep.* **2022**, *25*, 101303.
- [57] A. Kale, N. M. Rogers, *Cells* **2023**, *12*, 796.
- [58] E. Dondossola, B. M. Holzapfel, S. Alexander, et al., *Nat. Biomed. Eng.* **2017**, *1*, 0007.
- [59] J. R. Van Beijnum, E. J. M. Huijbers, K. Van Loon, A. Blanas, P. Akbari, A. Roos, T. J. Wong, S. S. Denisov, T. M. Hackeng, C. R. Jimenez, P. Nowak-Sliwinska, A. W. Griffioen, *Nat. Commun.* **2022**, *13*, 2842.
- [60] D. G. Barone, A. Carnicer-Lombarte, P. Tourlomousis, R. S. Hamilton, M. Prater, A. L. Rutz, I. B. Dimov, G. G. Malliaras, S. P. Lacour, A. A. B. Robertson, *Proc. Natl. Acad. Sci. USA* **2022**, *119*, e2115857119.
- [61] H. A. Zariwala, B. G. Borghuis, T. M. Hoogland, L. Madisen, L. Tian, C. I. De Zeeuw, H. Zeng, L. L. Looger, K. Svoboda, T.-W. Chen, *J. Neurosci.* **2012**, *32*, 3131.
- [62] E. Ilegems, P. P. Van Krieken, P. K. Edlund, A. Dicker, T. Alanentalo, M. Eriksson, S. Mandic, U. Ahlgren, P.-O. Berggren, *Sci. Rep.* **2015**, *5*, 10740.